Thickness dependence of anomalous Hall and Nernst effects in Ni-Fe thin films

Takumi Yamazaki,[1,2,*] Takeshi Seki,[1,2,3,†] Rajkumar Modak,[3] Keita Nakagawara,[3,‡] Takamasa Hirai,[3]
Keita Ito,[1,2] Ken-ichi Uchida,[1,2,3] and Koki Takanashi[1,2,4,§]
[1]*Institute for Materials Research, Tohoku University, Sendai 980-8577, Japan*
[2]*Center for Spintronics Research Network, Tohoku University, Sendai 980-8577, Japan*
[3]*National Institute for Materials Science, Tsukuba 305-0047, Japan*
[4]*Center for Science and Innovation in Spintronics, Core Research Cluster, Tohoku University, Sendai 980-8577, Japan*

(Received 7 April 2022; revised 22 May 2022; accepted 23 May 2022; published 13 June 2022)

We systematically investigate the Ni-Fe layer thickness (t) dependence of the anomalous Hall effect (AHE) and anomalous Nernst effect (ANE). The AHE and ANE show different behavior in the t dependence; the sign of the anomalous Hall resistivity changes around $t = 9$ nm, whereas the anomalous Nernst coefficient (S_{ANE}) keeps almost constant regardless of t, namely, no sign change of S_{ANE} with t. We analyze S_{ANE} and separate it into the contribution coming from the transverse thermoelectric conductivity (α_{xy}) and the AHE contribution coming from the Seebeck effect. The detailed analysis for S_{ANE} concludes that the AHE contribution is negligibly small and α_{xy}, which is related to the anomalous Hall conductivity (σ_{xy}) via the Mott relation, is also independent of t. To gain insight into the difference in the t dependence of σ_{xy} and α_{xy}, we clarify the origin of sign reversal in the AHE. The sign reversal in the AHE is attributed to the competing contribution of the different sources of the AHE: the extrinsic and intrinsic mechanisms. The present experimental finding of the difference between the t dependence on σ_{xy} and α_{xy} suggests that the relative degree between the extrinsic and intrinsic processes for the AHE is quite different from that for the ANE in the case of Ni-Fe.

DOI: 10.1103/PhysRevB.105.214416

I. INTRODUCTION

The anomalous Hall effect (AHE) [1] is one of the anomalous transport properties of a magnetic material, in which an applied electric current induces a transverse voltage depending on the direction of spontaneous magnetization. The origin of the AHE is the spin-orbit coupling, which brings the two types of mechanisms for the AHE: intrinsic and extrinsic. The former was proposed by Karplus and Luttinger [2] and recently explained using the Berry curvature of the Bloch wave [3]. The latter describes the asymmetric scattering for spin-up and spin-down electrons and is clarified to the two types: skew scattering [4,5] and side jump [6]. The AHE has been investigated both experimentally and theoretically in a variety of materials and plays a significant role for device applications [7–9].

The anomalous Nernst effect (ANE) is the thermoelectric counterpart of the AHE. The ANE refers to the generation of a transverse voltage in the cross-product direction of an applied temperature gradient and magnetization [10–12]. Since the ANE can achieve transverse thermoelectric generation, which has several advantages for thermoelectric applications, it has recently attracted broad attention as a promising energy harvesting technology [13–16]. To apply the ANE to practical thermoelectric devices, materials exhibiting the large anomalous Nernst coefficient S_{ANE} are required. Considering the resistivity tensor, S_{ANE} is expressed as

$$S_{\mathrm{ANE}} = \rho_{xx}\alpha_{xy} - \rho_{yx}\alpha_{xx}, \tag{1}$$

where ρ_{xx}, ρ_{yx}, α_{xx}, and α_{xy} refer to the longitudinal resistivity, anomalous Hall resistivity, longitudinal thermoelectric conductivity, and transverse thermoelectric conductivity, respectively [17]. Since α_{xy} is connected to the anomalous Hall conductivity σ_{xy} via the Mott relation, the relationship between the AHE and ANE is usually investigated for exploring materials with large S_{ANE} [17–23].

The Ni-Fe alloy known as permalloy (Py) is a representative material for spintronic devices [24–27]. A Py thin film shows a unique property for the AHE: the sign reversal of ρ_{yx} depending on its thickness [28–30]. Nevertheless, clear understanding of the reason behind the sign change of ρ_{yx} is still lacking. Although Chuang *et al.* [31] reported the thickness dependence of the ANE in Py thin film, the relationship between the thickness dependence of the AHE and ANE has not been discussed yet.

In this paper, we systematically investigate the thickness dependence of the AHE and ANE in Py thin films with different thicknesses. By exploiting a high-throughput screening technique, the anomalous Ettingshausen effect (AEE) [12,32–34], which is the reciprocal phenomenon of the ANE, is visualized for a Py film with a thickness gradient, showing that the anomalous thermoelectric property changes moderately

*takumi.yamazaki.d5@tohoku.ac.jp
†takeshi.seki@tohoku.ac.jp
‡Present address: Graduate School of Science, Tohoku University, Sendai 980-8578, Japan.
§Present address: Advanced Science Research Center, Japan Atomic Energy Agency, Tokai, Ibaraki 319-1195, Japan.

 ©2022 American Physical Society

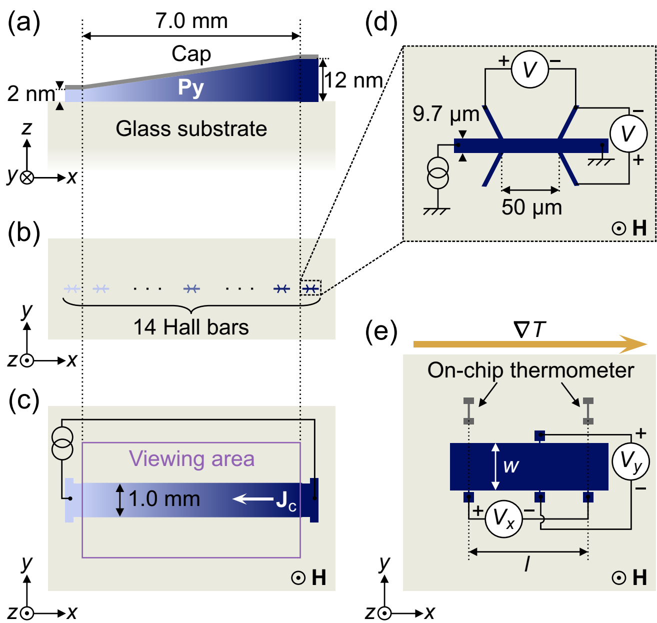

FIG. 1. Schematic illustrations of (a) the permalloy (Py) wedged film, (b) microfabricated pattern of Hall bars aligned in a wedged film for the electrical transport measurements, and (c) rectangular-shaped sample for the anomalous Ettingshausen effect (AEE) measurement using lock-in thermography (LIT). Schematic illustrations of (d) the Hall device structure and measurement setup and (e) the sample for the anomalous Nernst effect (ANE) and Seebeck effect (SE) measurements. **H**, $\mathbf{J}_c$, and ∇T denote the magnetic field, charge current, and temperature gradient, respectively.

with varying the thickness. The detailed analysis reveals that α_{xy} is almost independent of the thickness, which is different from the thickness-dependent behavior of the AHE. In addition, we clarify the origin of the sign reversal observed for the AHE by systematically investigating its temperature dependence.

II. EXPERIMENTAL DETAIL

The samples used in this paper were prepared using the following experimental procedure. Py thin films were grown on a glass substrate at room temperature using a RF magnetron sputtering with a base pressure of $< 1.0 \times 10^{-5}$ Pa and a process Ar gas pressure of 0.4 Pa. The composition of the sputtering target is $Ni_{81}Fe_{19}$. Two types of Py films were used for evaluating the thickness dependence of the AHE, ANE, Seebeck effect (SE), and AEE: wedged thin films with a thickness gradient and nonwedged thin films with a uniform thickness. The thicknesses of uniform films were set to be 5, 8, 10, and 12 nm. On the other hand, the thickness of wedged thin films was in the range of 2–12 nm over a length of 7.0 mm [see Fig. 1(a)]. Wedged thin films were fabricated by using a linear shutter that was moving at a constant speed of 0.18 mm/s during deposition. The Py layers were capped with the Al(1.5 nm)/Al-O(3.5 nm) layers for the AHE, ANE, and SE samples and with the Al(2 nm) layer for the AEE sample to prevent oxidation. The Al-O(3.5 nm) layers for the AHE, ANE, and SE samples were deposited by ion beam sputtering after breaking the vacuum. To investigate the thickness dependence of the AHE, the wedged sample was patterned into 14 aligned Hall bars with width of 9.7 μm and length of 50 μm through photolithography and Ar ion milling processes [see Figs. 1(b) and 1(d)]. Note that the thickness of a Hall bar is regarded as uniform due to the negligibly small thickness variation over its length. For the ANE and SE measurements, uniform thickness films were patterned into a Hall bar with the width of $w = 2.2$ mm and length of $l = 5.0$ mm through photolithography and Ar ion milling processes, as shown in Fig. 1(e). After etching, two Cr(10 nm)/Pt(150 nm) on-chip thermometers with their distance of l were fabricated by a lift-off process and ion beam sputtering. For the AEE measurement, as shown in Fig. 1(c), the wedged thin film was patterned into a rectangular shape with the width of 1.0 mm using a metallic shadow mask during the sputtering process.

Longitudinal and transverse electric and thermoelectric transport properties were evaluated using the Py films with various thicknesses. The longitudinal and transverse voltages were measured with the wedged Hall bar devices in the temperature range of 5–300 K using the physical properties measurement system (PPMS, Quantum Design, Inc.). In the AHE measurements, by applying an out-of-plane magnetic field **H** and a charge current in the longitudinal direction of the Hall bar, a transverse resistance R_{yx} was detected. The ANE measurements were performed using a homemade holder embedded in the PPMS. The transverse thermoelectric voltage V_y was measured by applying an out-of-plane magnetic field **H** and a temperature gradient ∇T in the longitudinal direction of the Hall bar, with a set temperature of 300 K. The actual device temperature is of a few Kelvins higher than the set temperature due to the sample heating. Subsequently, the temperature difference ΔT between the on-chip thermometers and ∇T $(= \Delta T/l)$ were carefully evaluated (see Appendix A for details). In this configuration, by measuring the longitudinal thermoelectric voltage V_x, the Seebeck coefficient S_{SE} was also obtained simultaneously. Note that the measured S_{SE} may include the contribution of the absolute Seebeck coefficient of the Al-1%Si bonding wire for electrical connection. To double check the thickness-dependent behavior of the SE, S_{SE} was also investigated by employing the Seebeck coefficient/electric resistance measurement system (ZEM-3, ADVANCE , Inc.) with the uniform-thickness Py films capped with the 2-nm-thick Al layer on 3 × 10 mm-sized glass substrates. The S_{SE} measurement using ZEM-3 was corrected considering the absolute Seebeck coefficient of the voltage probes.

To carry out the continuous investigation of the thickness dependence of anomalous thermoelectric properties, we employed the AEE measurement using lock-in thermography (LIT) [32,35–37] with the wedged thin film. In the AEE measurement, thermal images were obtained when a square-wave-modulated AC charge current with an amplitude of 4 mA, zero offset, and frequency of 5 Hz was applied along the x axis and an external magnetic field of 9 kOe was applied along the z axis [see Fig. 1(c)]. The pure AEE contribution was extracted from the raw LIT images using the procedure described in Refs. [38,39]. The sample surface was coated with insulating black ink to enhance the infrared emissivity.

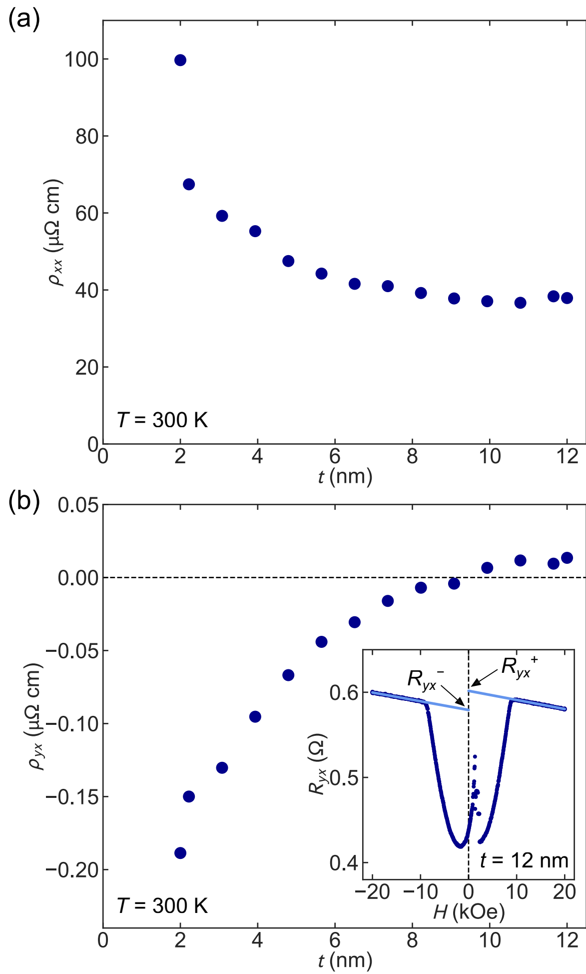

FIG. 2. Thickness t dependence of (a) the longitudinal resistivity ρ_{xx} and (b) the anomalous Hall resistivity ρ_{yx} in the Py thin film measured at 300 K. The inset of (b) shows the magnetic field H dependence of the transverse resistance R_{yx} for $t = 12$ nm.

The LIT measurement was performed at room temperature and atmospheric pressure.

III. RESULTS AND DISCUSSION

Figure 2 shows the Py layer thickness t dependence of ρ_{xx} and ρ_{yx} measured at 300 K. As shown in Fig. 2(a), ρ_{xx} increases with decreasing t, indicating that the finite size effect [40]. The inset of Fig. 2(b) shows the magnetic field H dependence of R_{yx} for $t = 12$ nm. The value of ρ_{yx} is derived from the relation $\rho_{yx} = t(R_{yx}^{+} - R_{yx}^{-})/2$, where $R_{yx}^{+(-)}$ are extrapolated from positive (negative) high magnetic field to zero magnetic field. Note that the large valley in the low-H region is attributed to the planar Hall effect [28,30,41]. As shown in Fig. 2(b), ρ_{yx} monotonically decreases with decreasing t, and the sign of ρ_{yx} is reversed from positive to negative around $t = 9$ nm. This sign change was reported in previous papers, but its origin has not fully been understood yet [28–30].

The measurement results of the SE and ANE are summarized in Fig. 3. Figure 3(b) shows the t dependence of S_{SE} with $t = 5$, 8, 10, and 12 nm. The blue (gray) plots in Fig. 3(b) denote S_{SE} of the microfabricated devices measured using the PPMS (the unpatterned blanket films measured using the ZEM-3). The values of S_{SE} of the microfabricated devices are derived from the slope of linear fit of V_x as a function of ΔT [also see Fig. 3(a)]. As shown in Fig. 3(b), the two different measurement techniques give almost the same values. It suggests that the contribution of the absolute Seebeck coefficient of the bonding wire is negligibly small in the S_{SE} measurement using the PPMS. Furthermore, S_{SE} measured by the two different techniques exhibits the same t-dependent behavior; the magnitude of S_{SE} monotonically decreases with decreasing t. This behavior is consistent with the effective mean free path model, in which the scattering at the surface and grain boundaries mostly determines the t dependence of S_{SE} [42]. Figure 3(c) presents V_y as a function of the magnetic field H for $t = 12$ nm. Since V_y saturates around $H = 9$ kOe, the dominant contribution of V_y is the ANE related to the magnetization of the Py film [43], whereas the contribution of the ordinary Nernst effect is negligibly small. The ANE-induced transverse electric field E_{ANE} is given by $E_{ANE} = V_{ANE}/w$, where V_{ANE} corresponds to the intercept of linear fit to V_y in the positive H region where the Py magnetization saturates. Then the value of S_{ANE} is evaluated from the slope of the linear fit to E_{ANE} as a function of ∇T [shown in the inset of Fig. 3(c)]. Figure 3(d) shows the t dependence of S_{ANE}, where the error bars represent the standard deviation of the linear fitting. As seen in Fig. 3(d), S_{ANE} is independent of t and keeps almost a constant value ($\sim 0.57\,\mu\mathrm{V\,K^{-1}}$), which is close to the result of the 10-nm-thick $Ni_{81}Fe_{19}$ film in a previous study [44].

Although we have roughly investigated the t dependence of S_{ANE} from Fig. 3(d), a further comprehensive investigation of anomalous thermoelectric properties is needed for the detailed comparison with the AHE. The AEE measurement for the wedged layer using LIT allows us to carry out a comprehensive study because the AEE is the reciprocal phenomenon of the ANE. In the perpendicularly magnetized configuration, the heat loss flowing from the Py film to the substrate affects the AEE-induced temperature change [32]. However, since the heat loss to the substrate is constant in the whole region of the Py film, the t dependence of the AEE can be obtained as the relative information. Hence, the visualization of the AEE-induced temperature change can be used to clarify the continuous information of the t dependence of S_{ANE}. In previous papers [39,45,46], the LIT imaging enabled the high-throughput screening of the composition dependence of spin-caloritronic effects using the composition-spread films fabricated by the combinatorial sputtering technique. In this paper, the LIT-based high-throughput screening was applied to the t dependence measurement of the AEE. Figures 4(a) and 4(b) display the lock-in amplitude A_{AEE} and phase ϕ_{AEE} images of the temperature modulation due to the AEE at $H = 9$ kOe, respectively. Note that the magnetic field of 9 kOe is similar or larger than the saturation field along the out-of-plane direction for the Py thin films at $t = 2$–12 nm [43]. These images were taken for the wedged Py layer with the rectangular shape, as illustrated in Fig. 1(c), in which t is continuously varied from 2 nm (left side) to 12 nm (right side). Black (white) dashed lines in Fig. 4(a) [Fig. 4(b)] indicate the

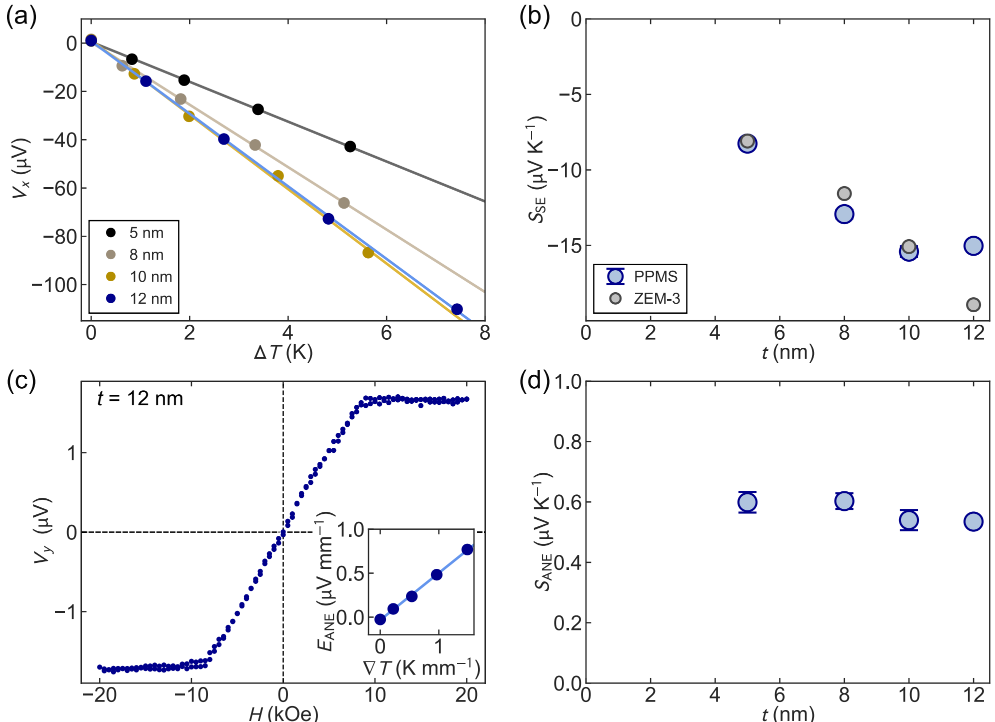

FIG. 3. (a) Longitudinal thermoelectric voltage V_x as a function of temperature difference ΔT for the 5-, 8-, 10-, and 12-nm-thick Py thin film measured at ~ 300 K. (b) Thickness t dependence of the Seebeck coefficient S_{SE} measured at ~ 300 K. Blue and gray plots denote S_{SE} measured for the microfabricated devices and the unpatterned blanket films, respectively. (c) Transverse thermoelectric voltage V_y as a function of magnetic field H for the 12-nm-thick Py thin film measured at ~ 300 K. The applied temperature gradient ∇T was set at $1.5\,\mathrm{K\,mm^{-1}}$. The inset of (c) shows the ∇T dependence of the anomalous Nernst effect (ANE)-induced transverse electric field E_{ANE} for the 12-nm-thick Py thin film. (d) t dependence of the anomalous Nernst coefficient S_{ANE} measured at ~ 300 K.

edge of the rectangular film. The A_{AEE} signal appears around the edge of the rectangular film, and the ϕ_{AEE} difference between the upper edge and lower edge is $\sim 180^\circ$. These behaviors indicate that heat generation (absorption) emerges at one (the other) edge of the film due to the in-plane heat current flowing edge to edge in the Py film, which is consistent with the symmetry of the AEE in the perpendicularly magnetized ferromagnetic metal [32]. Figure 4(c) plots the A_{AEE} signal as a function of t. The numerical values of the A_{AEE} signal were obtained by averaging the y-directional profile around the upper edge in Fig. 4(a), where the averaging width was defined as a full width at half maximum. While A_{AEE} shows almost a constant value in the range of $4\,\mathrm{nm} < t < 12\,\mathrm{nm}$, it gradually decays with decreasing t for $t < 4\,\mathrm{nm}$. The t-dependent behavior for $4\,\mathrm{nm} < t < 12\,\mathrm{nm}$ is qualitatively in agreement with the t dependence of S_{ANE} taken from Fig. 3(d). The t-dependent behavior for $t < 4\,\mathrm{nm}$ may be attributed to the change of the magnetic characteristic of the Py film [43]. Importantly, the A_{AEE} imaging indicates that S_{ANE} shows no drastic change around $t = 9\,\mathrm{nm}$, where the sign of ρ_{yx} is reversed. This is a clear experimental fact that the anomalous thermoelectric properties exhibit a totally different t dependence from that of the AHE.

To further clarify the t-dependent behavior of S_{ANE}, we analyze the ANE by separating the different origins of the transverse voltages due to the temperature gradients. As shown in Eq. (1), the heat-to-charge current conversion process for the ANE includes two contributions: the direct conversion of a temperature gradient to a transverse charge current via α_{xy} and the SE-driven transverse charge current through the AHE [17]. In the following, for simplicity, we denote the first and second terms of the right-hand side of Eq. (1) as $S_{\mathrm{I}}\,(= \rho_{xx}\alpha_{xy})$ and $S_{\mathrm{II}}\,(= -\rho_{yx}\alpha_{xx})$, respectively, where $\alpha_{xx}\,(= S_{\mathrm{SE}}/\rho_{xx})$ is the longitudinal thermoelectric conductivity. Figure 5(a) shows the t dependence of S_{I} and S_{II}. To determine the ρ_{xx} and ρ_{yx} values for calculating S_{I} and S_{II}, we used the linear interpolation for the data points of Figs. 2(a) and 2(b), respectively. As shown in Fig. 5(a), the S_{I} contribution is dominant for the Py films and almost independent of t in the range of 5–12 nm. Although the sign of S_{II} is reversed around $t = 9\,\mathrm{nm}$ due to the sign change of ρ_{yx} [see the inset of Fig. 5(a)], it does not affect the t dependence of S_{ANE} because the S_{II} contribution is negligibly small. As shown in Fig. 5(b), α_{xy} is independent of t and shows almost a constant value ($\sim 1.4\,\mathrm{A\,m^{-1}\,K^{-1}}$). This result suggests that the finite size effect does not appear in α_{xy} of the Py film in contrast with the other electric and thermoelectric transport properties (i.e., ρ_{xx}, ρ_{yx}, and S_{SE}).

Let us discuss the difference in the t-dependent behavior of α_{xy} and ρ_{yx}. Here, α_{xy} and σ_{xy} ($\sim \rho_{yx}/\rho_{xx}^2$ [47]) are correlated with each other via the Mott relation [22]:

$$\alpha_{xy} = -\frac{\pi^2}{3}\,\frac{k_{\mathrm{B}}^2 T}{e}\left(\frac{\partial \sigma_{xy}}{\partial \varepsilon}\right)_{E_{\mathrm{F}}}, \tag{2}$$

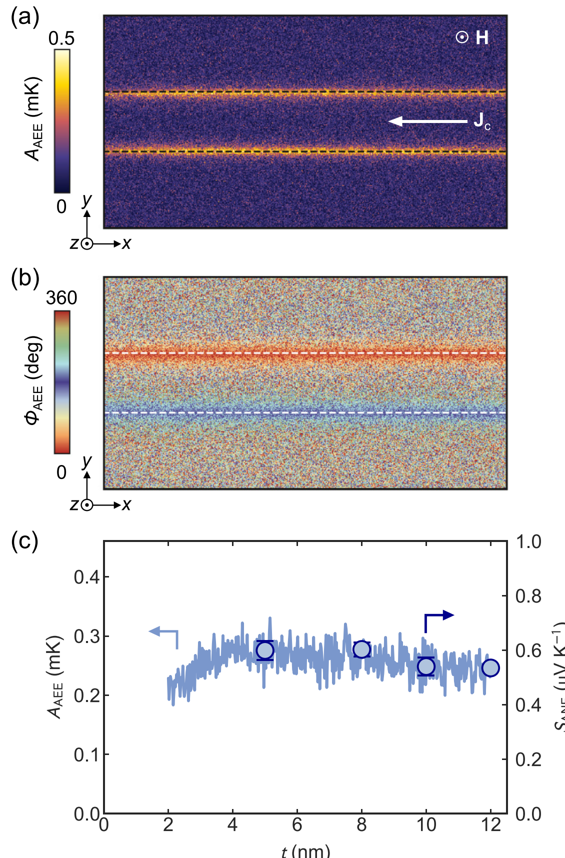

FIG. 4. (a) Lock-in amplitude $A_{\rm AEE}$ and (b) phase $\phi_{\rm AEE}$ images of the anomalous Ettingshausen effect (AEE)-induced temperature modulation. These images were taken for the wedged Py layer with the rectangular shape, in which the thickness t is continuously varied from 2 nm (left side) to 12 nm (right side). The black (white) dashed lines in (a) [(b)] denote the edges of the rectangular-shaped Py thin film. (c) t dependence of $A_{\rm AEE}$ and the anomalous Nernst coefficient $S_{\rm ANE}$. The numerical values of $A_{\rm AEE}$ are obtained by averaging the y-directional profile around the upper edge in (a), where the averaging width was defined as a full width at half maximum.

where $k_{\rm B}$ is the Boltzmann constant, and e is the elementary charge of electron. Here, $(\partial\sigma_{xy}/\partial\varepsilon)_{E_{\rm F}}$ is the energy derivative of σ_{xy} at the Fermi level $E_{\rm F}$. Also, ρ_{yx} (i.e., σ_{xy}) shows a sign reversal around $t = 9$ nm, whereas α_{xy} does not show a drastic change even with varying t. Considering these facts, elucidating the mechanism of sign change in ρ_{yx} is a way to understand the different t dependence between α_{xy} and ρ_{yx}. Then we clarify the origin of the sign change of ρ_{yx} in Py thin films by investigating the scaling relation between ρ_{xx} and ρ_{yx}.

The scaling relation for the AHE has been generally investigated to separate three mechanisms of the AHE: skew scattering, side jump, and intrinsic contributions [1]. In this paper, we introduced the scaling relation proposed by Hou *et al.* [48]:

$$\rho_{yx} = \alpha\rho_{xx0} + \beta_0\rho_{xx0}^2 + \gamma\rho_{xx0}\rho_{xxT} + \beta_1\rho_{xxT}^2, \tag{3}$$

where ρ_{xx0} is the residual resistivity due to static impurities and grain boundaries at low temperature (5 K in this paper),

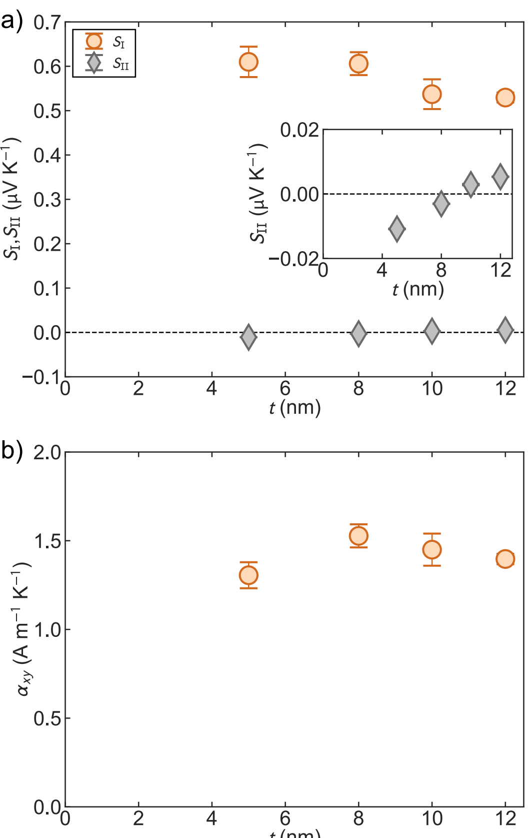

FIG. 5. Thickness t dependence of (a) $S_{\rm I}$ and $S_{\rm II}$ terms of the anomalous Nernst effect, which are denoted by orange circles and gray diamonds, respectively, and (b) the transverse thermoelectric conductivity α_{xy}. The inset of (a) shows the t dependence of $S_{\rm II}$ term.

and ρ_{xxT} $(= \rho_{xx} - \rho_{xx0})$ is the resistivity due to phonons. While α is the skew scattering angle due to static scattering sources including impurities and grain boundaries, the scaling parameters of β_0, γ, and β_1 are related to both side jump contributions due to static and dynamic (phonons) scattering sources and the intrinsic contribution. Thus, determining the four scaling parameters α, β_0, γ, and β_1 helps us to understand the mechanism of the AHE. Figure 6 shows the T dependence of ρ_{xx} and ρ_{yx} in the range of 5–300 K for the devices with different t. Here, ρ_{yx} around $t = 9$ nm (i.e., the thickness where the sign of ρ_{yx} is reversed) is independent of T [see Fig. 6(c)]. For better analysis, we introduce the scaling relation of σ_{xy}, the longitudinal conductivity σ_{xx} $(\sim 1/\rho_{xx}$ [47]), and residual longitudinal conductivity σ_{xx0} $(\sim 1/\rho_{xx0})$, which is obtained by rewriting Eq. (3) into

$$\sigma_{xy} = \alpha\sigma_{xx0}^{-1}\sigma_{xx}^2 + (\beta_0 + \beta_1 - \gamma)\left(\sigma_{xx0}^{-1}\sigma_{xx}\right)^2 + (\gamma - 2\beta_1)\sigma_{xx0}^{-1}\sigma_{xx} + \beta_1. \tag{4}$$

First, we determine the scaling parameter α related to the skew scattering. In the case of $T = 5$ K, i.e., $\sigma_{xx} \sim \sigma_{xx0}$, Eq. (4) reduces to $\sigma_{xy} = \alpha\sigma_{xx0} + \beta_0$ so that one can obtain α by using the experimental data of σ_{xy} and σ_{xx0}. Figure 7(a) shows σ_{xy} at 5 K as a function of σ_{xx0}. The value of σ_{xy} decreases with decreasing σ_{xx0} in the range of $t \geqslant 3.1$ nm and starts to increase

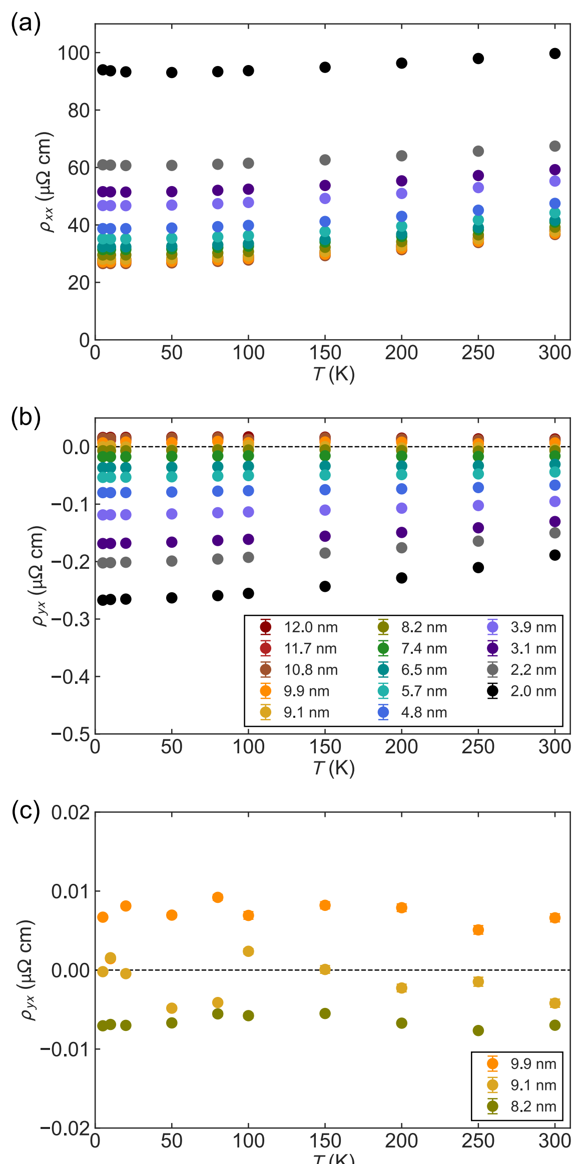

FIG. 6. Temperature T dependence of (a) the longitudinal resistivity ρ_{xx}, (b) the anomalous Hall resistivity ρ_{yx} for the various thicknesses, and (c) ρ_{yx} with $t = 8.2$, 9.1, and 9.9 nm.

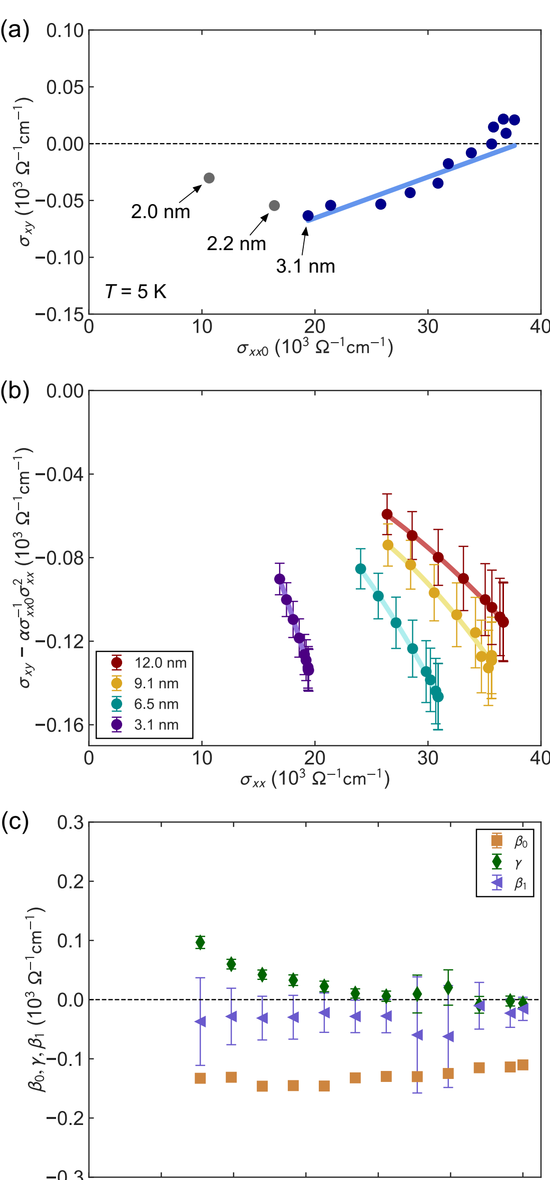

FIG. 7. (a) Anomalous Hall conductivity σ_{xy} as a function of residual longitudinal conductivity σ_{xx0} measured at 5 K. The blue line is the linear fit for $t \geqslant 3.1$ nm. (b) $\sigma_{xy} - \alpha\sigma_{xx0}^{-1}\sigma_{xx}^2$ as a function of σ_{xx} for the Py thin films with $t = 3.1$, 6.5, 9.1, and 12.0 nm. The solid lines are the fitted curves using Eq. (4). (c) Thickness t dependence of scaling parameters β_0, γ, and β_1.

below $t = 3.1$ nm, indicating that α drastically changes for ultrathin film. In the following, we focus on the experimental data in the range of $t \geqslant 3.1$ nm, in which α is regarded as the constant value. If the linear relation holds between σ_{xy} and σ_{xx0} for $t \geqslant 3.1$ nm, we obtained $\alpha = 0.36 \pm 0.05\%$, which is in good agreement with the value of the previous report ($\alpha = 0.32 \pm 0.1\%$) [30]. Subsequently, we determine the other scaling parameters of β_0, γ, and β_1. Figure 7(b) plots σ_{xy} as a function of σ_{xx} at various T and for various t. Note that the skew scattering term ($\alpha\sigma_{xx0}^{-1}\sigma_{xx}^2$) is subtracted from σ_{xy} using the obtained α. The solid lines in Fig. 7(b) represent the fitting curves with Eq. (4), and all the curves fit the experimental data well. Figure 7(c) shows the t dependence of β_0, γ, and β_1. While β_0 and β_1 keep almost constant regardless of t, γ gradually decreases with increasing t. Moreover, the values of γ and β_1 are clearly smaller than β_0, and β_0 is dominant in most thickness regions for $t > 5$ nm. This result suggests that the side jump contribution due to phonons is quite small compared with that of static scattering sources for $t > 5$ nm. Based on these facts, we focus on the scaling relation without phonon contributions. Then the original scaling of Eq. (3) becomes a simple form at 5 K, i.e., $\rho_{xxT} = 0$:

$$\rho_{yx} = \alpha\rho_{xx0} + \beta_0\rho_{xx0}^2. \quad (5)$$

The first term on the right-hand side of Eq. (5) means the skew scattering contribution, and the second term means the sum of the side jump contribution due to static scattering sources and the intrinsic contribution. In the following,

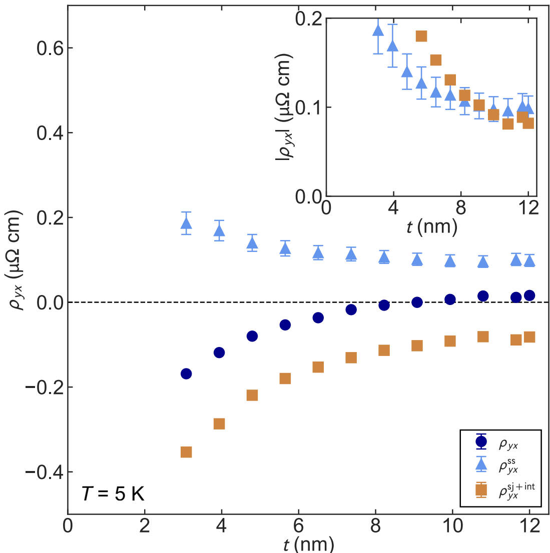

FIG. 8. Thickness t dependence of the anomalous Hall resistivity ρ_{yx}, ρ_{yx}^{ss}, and ρ_{yx}^{sj+int} at 5 K. The inset shows the t dependence of the absolute values of ρ_{yx}^{ss} and ρ_{yx}^{sj+int}.

we denote the first and second terms of the right-hand side of Eq. (5) as ρ_{yx}^{ss} $(=\alpha\rho_{xx0})$ and ρ_{yx}^{sj+int} $(=\beta_0\rho_{xx0}^2)$, respectively. Using ρ_{xx0} for various t, we obtained ρ_{yx}^{ss} and ρ_{yx}^{sj+int} as a function of t. Figure 8 summarizes the t dependence of ρ_{yx}, ρ_{yx}^{ss}, and ρ_{yx}^{sj+int} at 5 K. The t dependence of ρ_{yx} at 5 K shows almost the same as that at 300 K [see Fig. 2(b)]. As shown in Fig. 8, ρ_{yx}^{ss} and ρ_{yx}^{sj+int} exhibit signs opposite to each other. In addition, the magnitude of each monotonically decreases with increasing t and approaches a constant value. These facts indicate that the sign change of ρ_{yx} around $t = 9$ nm originates from the competing contributions of ρ_{yx}^{ss} and ρ_{yx}^{sj+int} with opposite signs; the contribution of ρ_{yx}^{sj+int} overcomes that of ρ_{yx}^{ss} with decreasing t (see the inset of Fig. 8). We also show the result of the analysis for ρ_{yx} at 300 K in Appendix B, which is based on Eq. (3). The analysis suggests that the sign change of ρ_{yx} is due to the α- and β_0-related terms even at 300 K, and the contributions of the β_1- and γ-related terms are quite small, which is consistent with the above discussion.

Finally, we refer to the roles of extrinsic and intrinsic contributions for the AHE and ANE of the present Py thin films. Earlier studies [49,50] suggested that the ANE also had different mechanisms like the AHE: the extrinsic contributions, i.e., skew scattering and side jump, and the intrinsic contribution. As discussed above, the extrinsic and intrinsic contributions are comparable in the AHE of Py, which causes the sign reversal of ρ_{yx} with t. On the other hand, the S_{I} term related to α_{xy} is dominant in the ANE of Py, and α_{xy} is almost independent of t. Although the amount of each contribution is unknown, these results suggest that the extrinsic and intrinsic contributions to α_{xy} are completely different from those to ρ_{yx}. It remains a challenge for future research to experimentally separate these contributions to α_{xy} and to clarify the strategy to enhance the ANE.

IV. CONCLUSIONS

This paper reported a comprehensive study on the t dependence of the longitudinal and transverse electric and thermoelectric properties in the Py thin films. While ρ_{yx} gradually decreases with decreasing t and its sign changed around $t = 9$ nm, S_{ANE} shows almost a constant value regardless of t. The LIT measurement of the AEE in the wedged film confirmed that S_{ANE} changes moderately even in the thickness region around $t = 9$ nm. In Py thin films, the S_{I} contribution is dominant, whereas the S_{II} contribution is negligibly small in the thickness range of 5–12 nm. α_{xy} is almost independent of t, indicating that the finite size effect does not appear remarkable in the t dependence of α_{xy}. To clarify the difference in the t-dependent behavior of ρ_{yx} and α_{xy}, the origin of the sign reversal in ρ_{yx} with varying t was investigated. The scaling relation between ρ_{xx} and ρ_{yx} led to the fact that the sign change in ρ_{yx} is due to the competing contribution of the skew scattering term and the sum of the side jump and intrinsic terms. These results suggest that the extrinsic and intrinsic contributions to α_{xy} and ρ_{yx} are apparently different in the Py film. Our results provide useful knowledge about the anomalous transport and thermoelectric properties for Py, which is a representative ferromagnetic material for many spintronic devices.

ACKNOWLEDGMENTS

The authors thank T. Sasaki for her help doing the film deposition by ion beam sputtering and R. Y. Umetsu for her help doing the transport measurement. The device fabrication was carried out at the Cooperative Research and Development Center for Advanced Materials, IMR, Tohoku University. This paper was supported by the JSPS KAKENHI Grant-in-Aid for Scientific Research (S) (Grant No. JP18H05246) and Grant-in-Aid for Scientific Research (A) (JP20H00299) and JST CREST "Creation of Innovative Core Technologies for Nano-enabled Thermal Management" (JPMJCR17I1). R.M. is supported by JSPS through the "JSPS Postdoctoral Fellowship for Research in Japan (Standard)" (P21064).

APPENDIX A: TEMPERATURE CALIBRATION FOR THE MEASUREMENT OF THE SE AND ANE

The measurement setup for the SE and ANE is shown in Fig. 9 [51]. The sample was fixed on two Cu blocks with thermal grease. A temperature gradient along the x direction was applied by heating one side of the Cu block using the chip heater, where the other side of the Cu block worked as the heat sink. We quantitatively evaluated the temperature difference ΔT and temperature gradient ∇T by the following procedure. When the thermoelectric voltage was measured, an AC charge current was also applied to the on-chip thermometers connected in series, and AC voltages of two thermometers (V_1 and V_2) were measured. By using the temperature coefficient of resistance for each on-chip thermometer, V_1 and V_2 were converted to the temperatures at the positions of thermometers T_1 and T_2, respectively. As a result, ΔT $(=T_2 - T_1)$ between the on-chip thermometers and ∇T $(=\Delta T/l)$ were obtained.

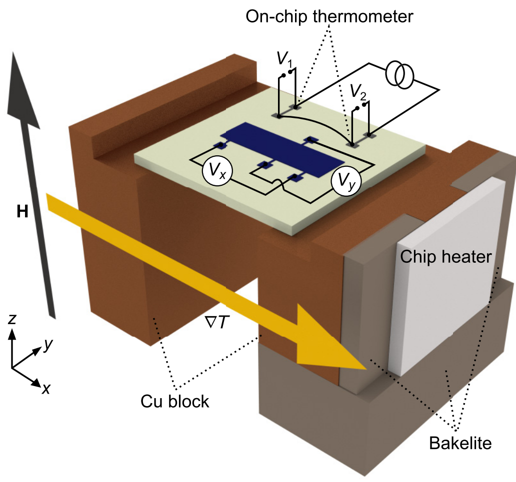

FIG. 9. Measurement setup for the Seebeck effect and anomalous Nernst effect. **H** and ∇T denote the magnetic field and temperature gradient, respectively.

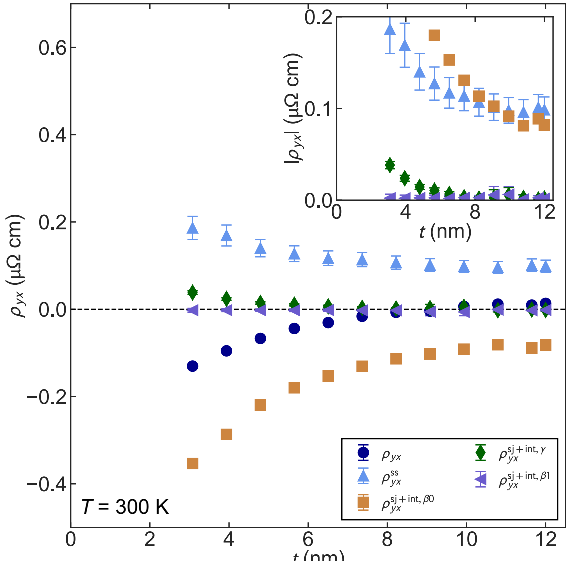

FIG. 10. Thickness t dependence of the anomalous Hall resistivity ρ_{yx}, $\rho_{yx}^{\rm ss}$, $\rho_{yx}^{\rm sj+int,\beta_0}$, $\rho_{yx}^{\rm sj+int,\gamma}$, and $\rho_{yx}^{\rm sj+int,\beta_1}$ at 300 K. The inset shows t dependence of the absolute values of $\rho_{yx}^{\rm ss}$, $\rho_{yx}^{\rm sj+int,\beta_0}$, $\rho_{yx}^{\rm sj+int,\gamma}$, and $\rho_{yx}^{\rm sj+int,\beta_1}$.

APPENDIX B: ANALYSIS OF THE THICKNESS DEPENDENCE OF THE ANOMALOUS HALL RESISTIVITY AT 300 K

We calculate the contributions of all scaling parameters to ρ_{yx} at 300 K. In a manner like Eq. (5), we denote the second, third, and fourth terms of the right-hand side of Eq. (3) as $\rho_{yx}^{\rm sj+int,\beta_0}$ $(=\beta_0\rho_{xx0}^2)$, $\rho_{yx}^{\rm sj+int,\gamma}$ $(=\gamma\rho_{xx0}\rho_{xxT})$, and $\rho_{yx}^{\rm sj+int,\beta_1}$ $(=\beta_1\rho_{xxT}^2)$, respectively. While $\rho_{yx}^{\rm sj+int,\beta_0}$ is the sum of the side jump contribution due to static scattering sources and the intrinsic contribution, $\rho_{yx}^{\rm sj+int,\gamma}$ and $\rho_{yx}^{\rm sj+int,\beta_1}$ include the phonon-induced side jump contribution. Figure 10 shows the t dependence of ρ_{yx}, $\rho_{yx}^{\rm ss}$, $\rho_{yx}^{\rm sj+int,\beta_0}$, $\rho_{yx}^{\rm sj+int,\gamma}$, and $\rho_{yx}^{\rm sj+int,\beta_1}$ at 300 K. The inset of Fig. 10 shows the t dependence of the absolute values of $\rho_{yx}^{\rm ss}$, $\rho_{yx}^{\rm sj+int,\beta_0}$, $\rho_{yx}^{\rm sj+int,\gamma}$, and $\rho_{yx}^{\rm sj+int,\beta_1}$. Comparing with $\rho_{yx}^{\rm ss}$ and $\rho_{yx}^{\rm sj+int,\beta_0}$, the contributions of $\rho_{yx}^{\rm sj+int,\gamma}$ and $\rho_{yx}^{\rm sj+int,\beta_1}$ are negligibly small. This result indicates that the sign change of ρ_{yx} is mainly determined by the magnitude of α- and β_0-related terms even at 300 K, and the β_1- and γ-related terms hardly affect the sign change of ρ_{yx}.

[1] N. Nagaosa, J. Sinova, S. Onoda, A. H. MacDonald, and N. P. Ong, Rev. Mod. Phys. **82**, 1539 (2010).
[2] R. Karplus and J. M. Luttinger, Phys. Rev. **95**, 1154 (1954).
[3] D. Xiao, M.-C. Chang, and Q. Niu, Rev. Mod. Phys. **82**, 1959 (2010).
[4] J. Smit, Physica (Amsterdam) **21**, 877 (1955).
[5] J. Smit, Physica (Amsterdam) **24**, 39 (1958).
[6] L. Berger, Phys. Rev. B **2**, 4559 (1970).
[7] Y. M. Lu, J. W. Cai, H. Y. Pan, and L. Sun, Appl. Phys. Lett. **100**, 022404 (2012).
[8] S. Nakatsuji, N. Kiyohara, and T. Higo, Nature (London) **527**, 212 (2015).
[9] E. Liu, Y. Sun, N. Kumar, L. Muechler, A. Sun, L. Jiao, S. Y. Yang, D. Liu, A. Liang, Q. Xu, J. Kroder, V. Süß, H. Borrmann, C. Shekhar, Z. Wang, C. Xi, W. Wang, W. Schnelle, S. Wirth, Y. Chen *et al.*, Nat. Phys. **14**, 1125 (2018).
[10] T. Miyasato, N. Abe, T. Fujii, A. Asamitsu, S. Onoda, Y. Onose, N. Nagaosa, and Y. Tokura, Phys. Rev. Lett. **99**, 086602 (2007).
[11] Y. Sakuraba, K. Hasegawa, M. Mizuguchi, T. Kubota, S. Mizukami, T. Miyazaki, and K. Takanashi, Appl. Phys. Express **6**, 033003 (2013).
[12] S. R. Boona, R. C. Myers, and J. P. Heremans, Energy Environ. Sci. **7**, 885 (2014).
[13] Y. Sakuraba, Scr. Mater. **111**, 29 (2016).
[14] M. Mizuguchi and S. Nakatsuji, Sci. Technol. Adv. Mater. **20**, 262 (2019).
[15] W. Zhou and Y. Sakuraba, Appl. Phys. Express **13**, 043001 (2020).
[16] J. Wang, A. Miura, R. Modak, Y. K. Takahashi, and K. Uchida, Sci. Rep. **11**, 11228 (2021).
[17] Y. Sakuraba, K. Hyodo, A. Sakuma, and S. Mitani, Phys. Rev. B **101**, 134407 (2020).
[18] H. Reichlova, R. Schlitz, S. Beckert, P. Swekis, A. Markou, Y. C. Chen, D. Kriegner, S. Fabretti, G. Hyeon Park, A. Niemann, S. Sudheendra, A. Thomas, K. Nielsch, C. Felser, and S. T. B. Goennenwein, Appl. Phys. Lett. **113**, 212405 (2018).
[19] A. Sakai, Y. P. Mizuta, A. A. Nugroho, R. Sihombing, T. Koretsune, M. T. Suzuki, N. Takemori, R. Ishii, D. Nishio-Hamane, R. Arita, P. Goswami, and S. Nakatsuji, Nat. Phys. **14**, 1119 (2018).
[20] A. Sakai, S. Minami, T. Koretsune, T. Chen, T. Higo, Y. Wang, T. Nomoto, M. Hirayama, S. Miwa, D. Nishio-Hamane, F. Ishii, R. Arita, and S. Nakatsuji, Nature (London) **581**, 53 (2020).
[21] Y. Hamada, Y. Kurokawa, T. Yamauchi, H. Hanamoto, and H. Yuasa, Appl. Phys. Lett. **119**, 152404 (2021).

[22] T. Seki, Y. Sakuraba, K. Masuda, A. Miura, M. Tsujikawa, K. Uchida, T. Kubota, Y. Miura, M. Shirai, and K. Takanashi, Phys. Rev. B **103**, L020402 (2021).
[23] Y. Pan, C. Le, B. He, S. J. Watzman, M. Yao, J. Gooth, J. P. Heremans, Y. Sun, and C. Felser, Nat. Mater. **21**, 203 (2022).
[24] F. J. Jedema, A. T. Filip, and B. J. van Wees, Nature (London) **410**, 345 (2001).
[25] K. Ando, S. Takahashi, K. Harii, K. Sasage, J. Ieda, S. Maekawa, and E. Saitoh, Phys. Rev. Lett. **101**, 036601 (2008).
[26] T. Yang, T. Kimura, and Y. Otani, Nat. Phys. **4**, 851 (2008).
[27] A. Hojem, D. Wesenberg, and B. L. Zink, Phys. Rev. B **94**, 024426 (2016).
[28] Y. Q. Zhang, N. Y. Sun, R. Shan, J. W. Zhang, S. M. Zhou, Z. Shi, and G. Y. Guo, J. Appl. Phys. **114**, 163714 (2013).
[29] R. Hao, J. Su, Q. Huang, T. Zhou, J. Cai, L. Bai, G. Han, S. Yu, G. L. Liu, S. Yan, and S. Kang, J. Magn. Magn. Mater. **478**, 187 (2019).
[30] Y. Omori, E. Sagasta, Y. Niimi, M. Gradhand, L. E. Hueso, F. Casanova, and Y. Otani, Phys. Rev. B **99**, 014403 (2019).
[31] T. C. Chuang, P. L. Su, P. H. Wu, and S. Y. Huang, Phys. Rev. B **96**, 174406 (2017).
[32] T. Seki, R. Iguchi, K. Takanashi, and K. Uchida, Appl. Phys. Lett. **112**, 152403 (2018).
[33] T. Seki, R. Iguchi, K. Takanashi, and K. Uchida, J. Phys. D: Appl. Phys. **51**, 254001 (2018).
[34] R. Das, R. Iguchi, and K. Uchida, Phys. Rev. Applied **11**, 034022 (2019).
[35] S. Daimon, R. Iguchi, T. Hioki, E. Saitoh, and K. Uchida, Nat. Commun. **7**, 13754 (2016).
[36] K. Uchida, S. Daimon, R. Iguchi, and E. Saitoh, Nature (London) **558**, 95 (2018).
[37] K. Uchida, M. Murata, A. Miura, and R. Iguchi, Phys. Rev. Lett. **125**, 106601 (2020).
[38] A. Miura, R. Iguchi, T. Seki, K. Takanashi, and K. Uchida, Phys. Rev. Materials **4**, 034409 (2020).
[39] R. Modak, K. Goto, S. Ueda, Y. Miura, K. Uchida, and Y. Sakuraba, APL Mater. **9**, 031105 (2021).
[40] E. H. Sondheimer, Adv. Phys. **50**, 499 (2001).
[41] K. L. Yau and J. T. H. Chang, J. Phys. F: Met. Phys. **1**, 38 (1971).
[42] C. R. Pichard, C. R. Tellier, and A. J. Tosser, J. Phys. F: Met. Phys. **10**, 2009 (1980).
[43] T. Seki, Y.-C. Lau, S. Iihama, and K. Takanashi, Phys. Rev. B **104**, 094430 (2021).
[44] T. Kikkawa, K. Uchida, S. Daimon, Y. Shiomi, H. Adachi, Z. Qiu, D. Hou, X.-F. Jin, S. Maekawa, and E. Saitoh, Phys. Rev. B **88**, 214403 (2013).
[45] K. Uchida, M. Sasaki, Y. Sakuraba, R. Iguchi, S. Daimon, E. Saitoh, and M. Goto, Sci. Rep. **8**, 16067 (2018).
[46] H. Masuda, R. Modak, T. Seki, K. Uchida, Y.-C. Lau, Y. Sakuraba, R. Iguchi, and K. Takanashi, Commun. Mater. **1**, 75 (2020).
[47] Considering the conversion of the resistivity tensor to the conductivity tensor, the longitudinal conductivity and anomalous Hall conductivity are derived from the relations $\sigma_{xx} = \rho_{xx}/(\rho_{xx}^2 + \rho_{yx}^2)$ and $\sigma_{xy} = \rho_{yx}/(\rho_{xx}^2 + \rho_{yx}^2)$, respectively. In the limit of $|\rho_{yx}| \ll |\rho_{xx}|$, σ_{xx} and σ_{xy} can be approximated as $\sigma_{xx} \sim 1/\rho_{xx}$ and $\sigma_{xy} \sim \rho_{yx}/\rho_{xx}^2$, respectively.
[48] D. Hou, G. Su, Y. Tian, X. Jin, S. A. Yang, and Q. Niu, Phys. Rev. Lett. **114**, 217203 (2015).
[49] J. Weischenberg, F. Freimuth, S. Blügel, and Y. Mokrousov, Phys. Rev. B **87**, 060406(R) (2013).
[50] M. Papaj and L. Fu, Phys. Rev. B **103**, 075424 (2021).
[51] J. Wang, Y.-C. Lau, W. Zhou, T. Seki, Y. Sakuraba, T. Kubota, K. Ito, and K. Takanashi, Adv. Elec. Mater. **2022**, 2101380 (2022).